EXPERIMENTAL INVESTIGATION AND MODELLING OF WATERFLOODING PERFORMANCE OF A BIOTURBATED CARBONATE FORMATION

I. Abu-Shiekah[1], S.K.Masalmeh[2] and X.D.Jing[2]
[1]Petroleum Development Oman (PDO) and [2]Shell Technology Oman (STO)

This paper was prepared for presentation at the International Symposium of the Society of Core Analysts held in Calgary, Canada, 10-12 September, 2007

ABSTRACT

In this paper we will address the impact of geological heterogeneity on waterflooding performance of a carbonate reservoir unit dominated by bioturbation. The methodology involves measurements of the basic rock properties from small core plugs taken within either the nodules or the base matrix as input to a detailed geological model at the scale of a Representative Element Volume (REV). Detailed fine-scale dynamic simulation is carried out with representative relative permeability and imbibition capillary pressure characteristics to mimic the physical waterflooding experiments at this scale. Distinctive saturation functions are assigned to the fine-scale grid blocks representing either the nodules or the base matrix. The efficiency of water flooding is investigated through sensitivity scenarios on formation rock/fluid parameters under representative field water injection conditions. It is found that the geological heterogeneity (i.e., bioturbation), the imbibition capillary pressure of the oil-wet carbonate and the viscous/capillary force balance (Nc) all have a strong impact on water-flooding recovery from this type of heterogeneous formation.

This paper also presents an upscaling methodology for both imbibition capillary pressure and relative permeability curves to account for the presence of nodules and the differing multi-phase flow characteristics between the matrix and nodules. The upscaled saturation functions can be used for sector- or field-scale simulations of the bioturbated units. The findings of this paper enable assessment of the impact of geological heterogeneity on water flooding when whole core flooding experiments are not available or when the nodular features are too large for whole cores to give Representative Element Volumes.

1. INTRODUCTION

The Natih formation is known to have a variety of geological heterogeneity at different length scales. One of the main features of the heterogeneity is the presence of reservoir sections dominated by bioturbated rocks (an example is shown in Figure 1). The rock fabric is made of nodular and matrix texture and heterogeneous in the centimeter-scale. Often the nodules are surrounded by either leached or cemented thin regions. Visual inspection of retrieved reservoir cores indicates likely property variations within the rock. This is further confirmed by measurements of petrophysical properties such as permeability, porosity and multi-phase flow characteristics of the matrix and nodules.

This type of geological heterogeneity has a strong impact on both the effective pore volume (hence STOIIP) and the effective fluid flow properties (hence production and recovery) of the formation. The presence of nodules leads to different porosity and permeability classes within the bioturbated unit, as well as different capillary pressure (in drainage and imbibition) and relative permeability characteristics which need to be assigned in fine-grid simulations. The variation of both static and dynamic properties needs to be taken into account in upscaling from fine-grid models (which represent the matrix and nodule properties explicitly) to coarse-grid models (where upscaled static and dynamic flow properties need to be used).

The impact of this scale of geological heterogeneity on waterflooding performance is investigated through detailed core characterization and flow simulation to represent both matrix and nodule properties as two different rock types in the unit. A series of water-flooding experiments have been simulated at the whole-core scale and above where both matrix and nodular features and properties are distributed spatially according to that observed in Natih core and outcrop analogues.

2. ROCK CHARACTERISATION

Porosity and Permeability Distributions

Figure 1 shows a photo of a typical bioturbated core which is composed of at least two distinctive porosity and permeability classes, referred to as the matrix (higher porosity and permeability) and the nodules (lower porosity and permeability). A mini-permeameter was used on the whole core samples to measure the permeability distribution as shown in Figure 2. The mini-permeameter measurements are only indicative of the permeability variations due to the limitations of the measurement technique, e.g., possible surface irregularities and contamination, and the variations of possible remaining hydrocarbon saturations in the pore space. Nevertheless the measurements show that the permeability variations can be as large as two orders of magnitude.

To assess the porosity variations on the bioturbated rock, a piece of core material was scanned in the CT scanner. The images were taken for a series of cross-sectional planes (2mm spacing) perpendicular to the axis of the core. The scanning pictures shown in Figure 3 indicate that the nodular features in the sample have 3D features as observed in the analogue Natih outcrop rock. Subsequently small plugs were taken from the core material and whenever possible several homogeneous plugs that are representative of either the nodules or the matrix were drilled. The small plugs were chosen to have adequate sizes to enable standard routine measurements on the samples. The optimal plugs obtained for the given core material were of 1 cm in diameter and 1 cm long and used in porosity, permeability and mercury-air capillary pressure measurements. For other Natih units where nodular features may be different in sizes, core plugs of appropriate sizes need to be taken for petrophysical and flow measurements which may

pose SCAL challenges in case of the relatively small average nodule sizes. In total 24 plugs (as homogeneous as possible representing either matrix or nodule) were drilled and cleaned, followed by porosity and gas permeability measurements. The measured porosity distribution indicates a porosity range from 0.10 to 0.45, which can be grouped into two porosity classes: 0.15-0.20 for the nodules and 0.30-0.40 for the matrix.

The air permeability was measured for 17 samples and shows two orders of magnitude of permeability variations across the matrix and nodules. The cross-plot of the permeability vs. porosity relationship is shown in Figure 4. It is noted that the general trend of the permeability vs. porosity curve is consistent with the typical core analysis data (of regular 1-1.5 inch plugs) from the Natih formation. In general some Natih formation porosity-permeability scatter (not shown here) may be caused by the relatively small fraction of either the matrix material in nodule plugs or the nodule material in matrix plugs.

Primary Drainage Capillary Pressure

After the porosity and permeability measurements, mercury-air capillary pressure curves were measured on the small plug samples. The measurements as shown in Figure 5 reveal two distinctive groups of capillary pressure curves: one for the matrix (the high porosity class) and the other for the nodules (low porosity class). The mercury-air capillary pressure data were then converted to the corresponding brine-crude system taking into account the interfacial tension and contact angle ($\sigma.\cos(\theta)$) for the specific brine-crude system. The capillary pressure curves show significant impact on the initial oil saturation especially in the layers close to the free water level.

In this study, the data were synthesized into two representative primary drainage curves, one for matrix and the other for nodules as shown in Figures 5 & 6. In general, further scaling of capillary pressure with permeability and porosity within each rock type (nodules and base matrix) following the Leverett-J type of approach can be made.

Imbibition Capillary Pressure and Relative Permeability

Due to the small size of the selected plugs, the imbibition capillary pressure curves were not measured directly on all the selected samples. The cored matrix and nodule plugs in general did not have adequate sizes suitable for multi-phase flow and centrifuge measurements to represent the matrix and the nodules separately.

Since the two rock types have different porosity, permeability and primary drainage data, they are expected to have different imbibition capillary pressure curves. No spontaneous imbibition of water was observed on samples from the reservoir under study following wettability restoration (Mookerjee and Alias, 2006), and in general low (< 20%) residual oil saturation was found for both rock types. Recently it has been reported that the imbibition capillary pressure for samples showing no spontaneous imbibition, which is generally the case for limestone oil reservoirs, may be calculated from the corresponding primary drainage capillary pressure (Masalmeh and Jing, 2006). The procedure requires

certain SCAL experiments to constrain both the contact angle hysteresis and trapping functions (e.g., residual oil saturations). For the base case model in this study the contact angle in the waterflooding imbibition was set based on the regional SCAL database. Scenarios were run for a range of imbibition contact angles/wettability cases ($\cos(\theta)$ = -0.8, -0.6, -0.5, -0.4 and 0.0). The residual oil saturation was varied from 0.05 – 0.10 for the matrix and 0.15 - 0.20 for the nodules in the simulation. An example of the resulting water/oil imbibition capillary pressure curves is shown in Figure 6.

The relative permeability model is based on several previous studies on Natih formation samples. The residual oil saturations for matrix and nodules are set to be consistent with the corresponding imbibition capillary pressure curves. The imbibition relative permeability curves are generated using the parameters in Table 1.

Table 1: Corey relative permeability parameters for the matrix and nodules.

	S_{wc}	S_{or}	N_o	N_w	Kro	Krw
Nodules	0.05	0.2	3.5	2.8	0.8	0.6
Matrix	0.05	0.1	3.5	2.7	0.8	0.8

3. NUMERICAL SIMULATIONS

Model Setup

In the numerical water-flooding experiment, the model core was constructed in a Cartesian grid system. NX=NY=20 & NZ=40 were used for a model core of 10 cm in diameter and 20 cm long for the sensitivity study. For the average nodule size encountered in this study, a model size of 20 cm in diameter and 40 cm long was constructed and used in the upscaling to allow a Representative Element Volume (REV) to be approached. The first and last grid blocks in the Z-direction are dummy layers (not part of the core) to mimic the physical experiment of injection and production. The boundary conditions were set such that the injector is mimicked with a constant flux boundary condition at the plane Z=1 and the producer as a pressure boundary condition (1 Bar) at the plane Z =NZ.

The porosity map was generated to resemble the images obtained from a section of bioturbated samples. The nodules are distributed randomly in three dimensions and are isolated from each other by the matrix until a certain volume fraction of the nodules is reached at that point they can be in touch. An example 3D “core” model is shown in Figure 7 for the case of 40% nodules volume. The permeability of each grid block was calculated according to the permeability-porosity relation shown in Figure 4.
The effective permeability of the entire core model was obtained from the Darcy’s Law after solving for the total flow rate under the given pressure drop across the model.

Model Initialization
The model is initialized hydrostatically based on capillary and gravitational equilibrium with the assumption that both nodules and matrix are filled to the connate water.

Typical water injection rates as in the relevant field pilots were used. The capillary/viscous force balance has been taken into account with the capillary number term $N_c=(\mu.\nu/\sigma)$ where σ is the interfacial tension, μ is the viscosity and ν is the flow velocity. Injection flow rate corresponding to ν ~0.4 ft/day field rate was used in the base case but other rate sensitivities were investigated within the capillary dominance ($Nc < 10^{-6}$) region. In the steady-state experiment, a much higher injection rate was used to demonstrate the effect of flow-rate (hence Nc) on the recovery efficiency of this type of heterogeneous carbonates. A single-speed centrifuge experiment was also simulated to compare against the high rate steady-state experiment on the bioturbated REV.

4. SIMULATION RESULTS

Figure 8 shows the waterflood simulation results as a function of pore volume injected (corresponds to a field velocity of ~0.4 ft/day). As expected, the total recovery factor decreases as the percentage of the nodules volume increases due to the water bypassing and hence more oil remaining in the nodules. Next the imbibition capillary pressure models were changed for both the nodules and the matrix by the imbibition $\cos(\theta)$ multiplier from the base case $\cos(\theta) = -0.5$ to a range of values reflecting varying degrees of oil-wetness: -0.8, -0.6, -0.4 and 0.0. The same primary drainage and relative permeability as in the base case were used. The case of ($\cos(\theta)=0$) i.e., zero imbibition capillary pressure for both the matrix and nodules shows a better recovery factor compared to the oil-wet base case of $\cos(\theta) = -0.5$ (Figure 9).

The imbibition capillary pressure variation between the nodules and the matrix are the key factor in explaining the observed recovery behaviour. In all of the above sections a constant injection rate was used (corresponding to about 0.4 ft/day). A comparison of the injection flow rates of $\nu \sim 0.04$ ft/day & $\nu \sim 4$ ft/day with the base case of $\nu \sim 0.4$ ft/day on the recovery factor is shown in Figure 10. The contribution to the total recovery factor from the nodules is reduced when the injection flow rate decreases as the capillary forces (especially the negative entry pressure of the oil-wet nodules) dominate the flow behaviour. The capillary number distribution shows typically three orders of magnitude difference between the nodules and the matrix. The effect of gravitational force is generally negligible compared to the capillary and viscous forces for the given model.

5. UPSCALING FOR STATIC AND DYNAMIC PROPERTIES

Fine-grid simulation is necessary to represent the static and dynamic properties correctly for both the base matrix and the nodules at the cm-scale. However, for field-scale simulations where grid-block sizes are in the order of meters to 10's of meters, both static and dynamic upscaling is needed to derive effective properties for the coarser grid blocks.

The so-called static upscaling (i.e., to derive average grid-block porosity, permeability and saturations) is a solved problem. In this section we focus on the upscaling of capillary pressure and relative permeability curves from the fine-grid scale to the coarse-grid scale typically used for this type of carbonate formations. The capillary pressure upscaling can be done analytically while the relative permeability upscaling for a range for viscous/capillary force balances is carried out by numerical simulation.

Upscaling Capillary Pressure

We first present an analytical upscaling procedure of capillary pressure curves for both drainage and imbibition processes based on the concept of capillary equilibrium. The technique can be applied for systems of any number of capillary pressure curves representing different rock types. In this procedure, the water saturation is expressed as a function of capillary pressure, $S_w(P_c)$. The upscaled water saturation for a given P_c value can be calculated from pore volume averaging, using the following equation:

$$S_w^{upscaled}(P_c) = \frac{\sum_{j=1}^{n} S_{wj}(P_c) * \varphi_j * V_j}{\sum_{j=1}^{n} \varphi_j * V_j}$$

where φ_j is the porosity of rock type (j), V_j is the volume fraction of rock type (j) and $S_{wj}(P_c)$ is the water saturation vs. capillary pressure function of rock type (j). For a system of two different Pc curves, e.g., one for the nodules (n) and another for the matrix (m), the upscaled water saturation vs. capillary pressure function can be expressed as:

$$S_w^{upscaled}(P_c) = \frac{S_{wn}(P_c) * \varphi_n * V_n + S_{wm}(P_c) * \varphi_m * V_m}{\varphi_n * V_n + \varphi_m * V_m}$$

where the subscript (n) represents the *nodules* and the subscript (m) represents the *matrix*. The same procedure can be used for both drainage and imbibition Pc curves. Figure 11 shows the upscaled drainage and imbibition capillary pressure curves, in comparison with the matrix and nodule capillary pressure curves.

This analytical technique was used to verify the numerical upscaling procedure where a centrifuge "experiment" was firstly simulated using a fine-grid model to give production profiles for each centrifuge speed. This numerical centrifuge experiment was performed on a heterogeneous whole core model consisting of 40% nodules and 60% matrix volume. The Pc curves for matrix and nodules shown in Figure 11 have been used as input in the multi-speed centrifuge 3D numerical experiment. Secondly, the water and oil productions in the above-mentioned numerical experiment were history-matched by treating the system as a 1D "homogenous" model (at the REV scale). The average porosity was calculated as 28% and the effective permeability was calculated numerically as 4.7 mD. The primary drainage and imbibition capillary pressures derived by history-matching this bioturbated model core under centrifuge were in perfect agreement with the

analytical solutions derived as shown in Figure 11. This agreement of analytical vs. numerical solutions for upscaling capillary pressure also validates the use of centrifuge experiments for heterogeneous core plugs.

Upscaling Relative Permeability

The relative permeability at the REV scale for both water and oil is derived through a numerical steady-state experiment. Similar to the numerical centrifuge experiments described above, the first step is to construct a fine-grid model where the static properties and dynamic imbibition capillary pressure and relative permeability characteristics of the nodules and matrix were represented explicitly in the fine grids. A numerical steady-state experiment is then simulated in the forward modelling mode to generate the water and oil production and pressure drops for a range fractional flow steps. During the numerical experiments the total flow rates were varied to correspond to 0.2, 0.4, 4 and 40 ft/day field rates, respectively. The 40 ft/day case has a viscous pressure gradient high enough to overcome capillary end effect in the numerical experiments.

The next step in the upscaling is to calculate the effective static and dynamic properties of the model core by treating it as a "homogeneous" 1D sample. The upscaled porosity, permeability (including the end-point oil and water phase permeabilities) and saturation are calculated for the 1D model. The numerically simulated steady-state experiments for a range of fractional-flow and total-rate conditions mentioned above are then history-matched by (1) inputting the upscaled capillary pressure curves described in the above section as a given; (2) adjusting both the oil and water relative permeabilities (except for the end points where the solutions are available via the pressure-solver method) until a close match of water and oil production profiles and pressure drops is achieved. Numerical experiments were also carried out to investigate the use of a dummy core with varying lengths at the outlet end to suppress the capillary end-effect, and a scaling rule was used to indicate the condition when the relative permeability can be calculated analytically from the Darcy's law without the need of numerical simulation to account for the capillary pressure effect.

The upscaled relative permeability curves are shown in Figure 12 for the three different injection rates (hence capillary number Nc) indicated in the figure. The results show a clear dependency of derived relative permeability at the REV scale on the injection rates (hence the Nc) for this bioturbated rock. Similar behaviour of Nc dependency was also reported by Coll et al. (2001) for bioturbated sandstone rocks with different wettability characteristics. Numerical experiments were also run in the single-speed centrifuge mode to derive the upscaled oil relative permeability (as water relative permeability cannot be derived from single speed imbibition centrifuge experiment). The single-speed centrifuge gives the same oil relative permeability as the highest injection rate case in the steady-state experiment (as shown in Figure 12) where the negative imbibition capillary pressure for the nodules is overcome by the viscous force thus allowing oil to be swept from the nodules. Figures 13 & 14 show the remaining oil saturation and capillary number

distributions at the fine scale, respectively, after waterflooding a bioturbated model at 0.4 ft/day.

6. DISCUSSION

In this paper, the waterflood recovery factor was studied as a function of the nodules volume fraction in the bioturbated system. Two different saturation functions have been assigned in the fine-grid simulation, one for the nodules and one for the matrix. The same procedure can be used for systems of more than two different rock types where each rock type may have a different set of saturation functions (Pc and relative permeability curves). For example, it was observed in the reservoir rock that the interface between the nodules and the matrix is leached. The impact of the leached rims on fluid flow can be assessed using a system of three different rock types (nodules, matrix and rims) following the same methodology presented in this paper.

The effect of the presence of nodules on recovery factor is attributed to the contrast between the nodules and the matrix capillary pressure curves (Masalmeh et al, 2003), and the balance of capillary/viscous force balance as the gravitational force is relatively insignificant at this scale. This force balance can be properly captured by using the capillary number (Nc) scaling. Other parameters such as relative permeability and residual oil saturation also influence the total recovery factor which is the sum of the individual contributions from the nodules and the matrix.

Carbonate reservoirs are heterogeneous at all scales and therefore upscaling is necessary to properly model water flooding in full-field and sector-scale simulation studies. Upscaling of static and dynamic properties presented in this paper relies on careful core measurements on small-size plugs to represent the matrix and nodules petrophysical and flow properties accurately. Fine-grid simulation is then conducted to capture the correct flow physics and boundary conditions representative for field applications. This methodology is an effective approach to account for the effect of heterogeneity on water flooding performance and the related upscaling to derive static and dynamic properties for field applications. Further work in ongoing to construct the static model with more realistic 3D geometries of the nodules using CT and statistical means.

In the case where the nodules are too small to be cored and measured separately, it is recommended that physical water-flooding experiment of whole-core scale under field representative rate conditions be conducted. The detailed numerical or “virtual” experiments with the associated upscaling procedure present a useful approach for this type of heterogeneous carbonates. It is also the only possible method for the bioturbated units where nodules are so large that whole-core may not capture a Representative Element Volume (REV) to allow meaningful measurements for both static and dynamic properties.

7. CONCLUSIONS

The following conclusions can be drawn based on this paper:

1. Both experimental measurements and numerical simulations were conducted to assess the impact of heterogeneity (centimetre-scale bioturbation) on water flooding performance and its subsequent upscaling.
2. The total recovery factor is strongly dependent on the contrast between the oil-wet (negative) imbibition capillary pressure of the nodules and the matrix, the relative permeability and the injection flow rates.
3. When a representative field rate is applied, a relatively low recovery factor is achieved from the nodules as compared to the matrix due to the imbibition capillary pressure contrast between the base matrix and the nodules and hence water by-passing the nodules.
4. A practical methodology is presented for obtaining upscaled effective static and dynamic properties of this type of heterogeneous carbonate formations, combining experimental measurements of small matrix and nodules plugs with detailed fine-grid numerical simulation.
5. An analytical procedure is presented to upscale capillary pressure curves (both drainage and imbibition). A new procedure is also presented to upscale relative permeability using steady-state numerical experiments and simulation history match taking into account the capillary pressure functions. The upscaled saturation functions can be used in sector- and field-scale simulations based on the capillary number (Nc) scaling.
6. It is found that the upscaled relative permeability curve shows a strong rate (Nc) dependency, as waterflooding at higher rates lead to an increase in oil recovery from the nodules. This also presents an interesting opportunity for improving oil recovery from this type of heterogeneous carbonates using means other than rate increase to modify the capillary number and improve sweep efficiency.

ACKNOWLEDGEMENTS

We thank the Ministry of Oil & Gas of Oman for granting permission to publish this paper. We also would like to thank our colleagues in Petroleum Development Oman (PDO) and Shell Technology Oman (STO) for stimulating discussions.

REFERENCES

Coll, C., Muggeridge, A. and Jing, X.D. **"**Regional Upscaling: A New Method to Upscale Waterflooding in Heterogeneous Reservoirs for a Range of Capillary and Gravity Effects**".** SPE 59337, SPE Journal, p.299-310, September, (2001).

Maas, J.G. and Schulte A.M.: "Computer Simulation of Special Core Analysis (SCAL) Flow Experiments Shared on the Internet", SCA-9719, in Proceedings of the International Symposium of the Society of Core Analysts, Calgary, Canada (1997).

Masalmeh, S.K. and Jing, X.D: "Capillary Pressure Characteristics of Carbonate Reservoirs: Relationship between Drainage and Imbibition Curves". SCA2006-16, in Proceedings of the International Symposium of the Society of Core Analysts, Trondheim, Norway, 12-16 September, (2006).

Masalmeh, S. K., Jing, X.D. van Vark, W., Christiansen, S. van der Weerd, H. and van Dorp, J. "Impact of SCAL on Carbonate Reservoirs: How Capillary Forces Can Affect Field Performance Predictions". SCA2003-36, in Proceedings of the International Symposium of the Society of Core Analysts, Pau, France, 21-24, September, (2003).

Mookerjee, A. and Alias, Z. A.: "Core Analysis Program For A Giant, Complex Fractured Carbonate Field In Oman: Learnings And Key Results". SCA2006-19, in Proceedings of the International Symposium of the Society of Core Analysts, Trondheim, Norway, 12-16 September, (2006).

Figure 1: A photo from a bioturbated core taken from the Natih formation.

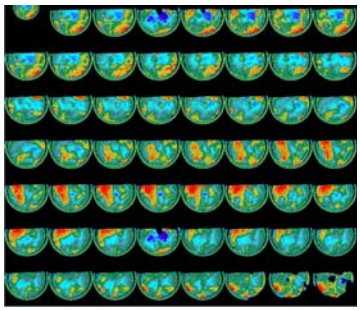

Figure 3: CT images of the core samples taken eve 2mm perpendicular to core axis (warm color indicat tighter rock nodules).

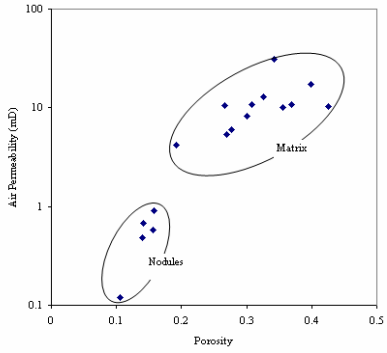

Figure 4: Air permeability vs. porosity of the plugs

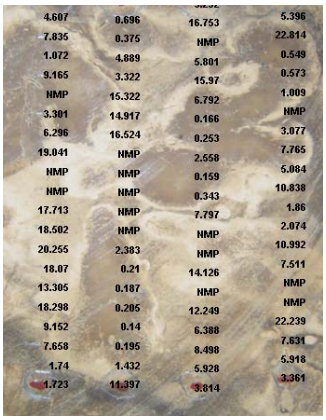

Figure 2: An example mini-permeameter measurement on Natih formation core. The permeability unit is in mD. NMP refers to "no measurement possible".

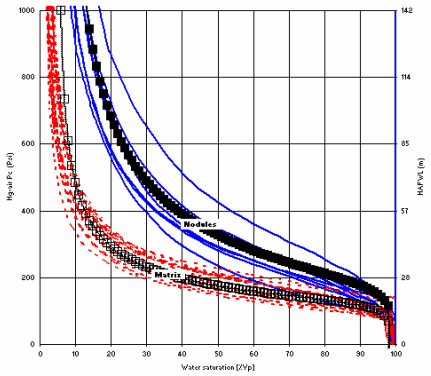

Figure 5: Mercury-air capillary pressure curves for both the matrix (red-dotted) and the nodules (blue-solid) and corresponding heights above free water level (HAFWL).

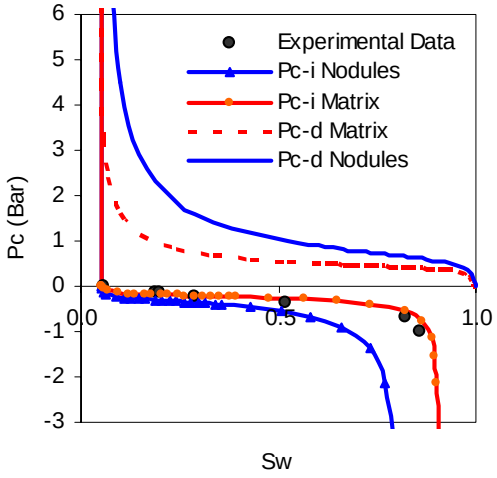

Figure 6: Primary drainage (Pc-d) and imbibition (Pc-I) capillary pressure curves for both the nodules and the matrix. The symbols are experimental imbibition data of a matrix sample.

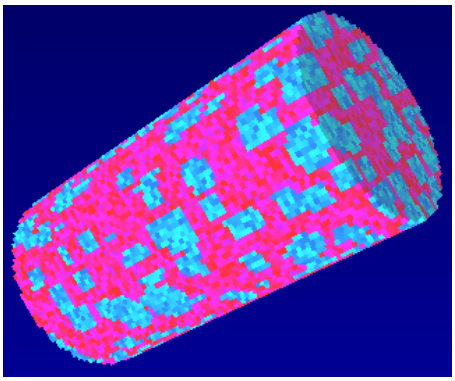

Figure 7: Three-dimensional porosity map for the case of 40 % nodules volume. The REV core size is 40 cm long and 20 cm in diameter.

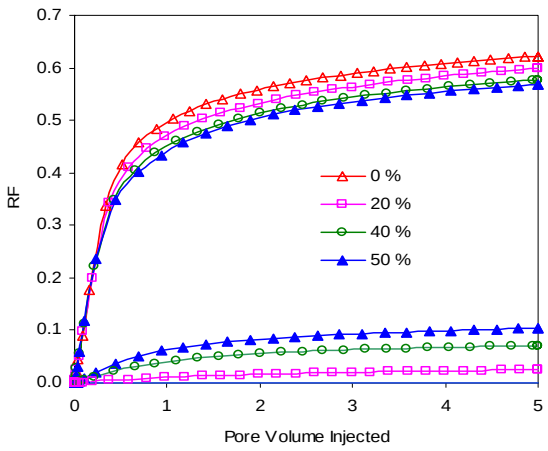

Figure 8: The total recovery factor as a function of the injected pore volumes for different nodules volume percentage (from 0 % up to 50 %). The injection flow rate corresponds to 0.4 ft/day. The lower curves are the contribution from the nodules to the total RF.

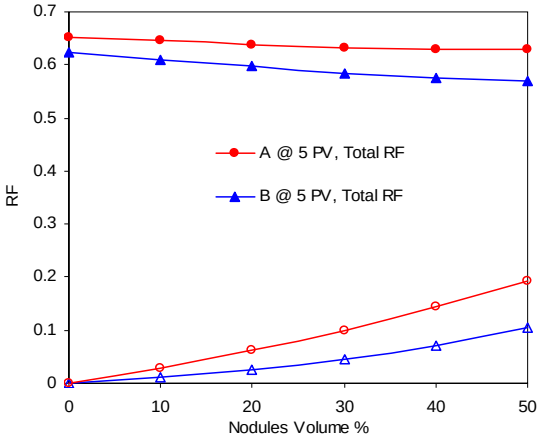

Figure 9: The total recovery factor as a function of the nodules volume percentage for two different capillary pressures after five pore volumes injected. A refers to $\cos(\theta)=0$ and B refers to $\cos(\theta)=-0.5$. The lower curves (with empty circles) are the nodules contribution to the total RF.

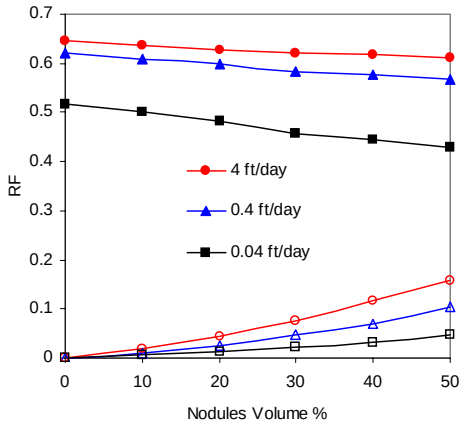

Figure 10: Recovery factor after 5 PVs injected vs. nodules percentage for three water injection rates. The open symbols indicate the nodules contribution to RF.

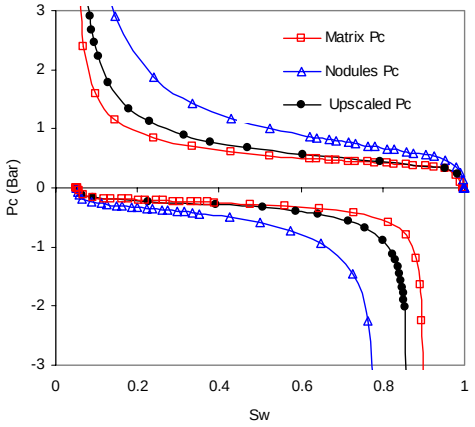

Figure 11: The drainage and imbibition capillary pressure curves for matrix, nodules and upscaled for the whole unit.

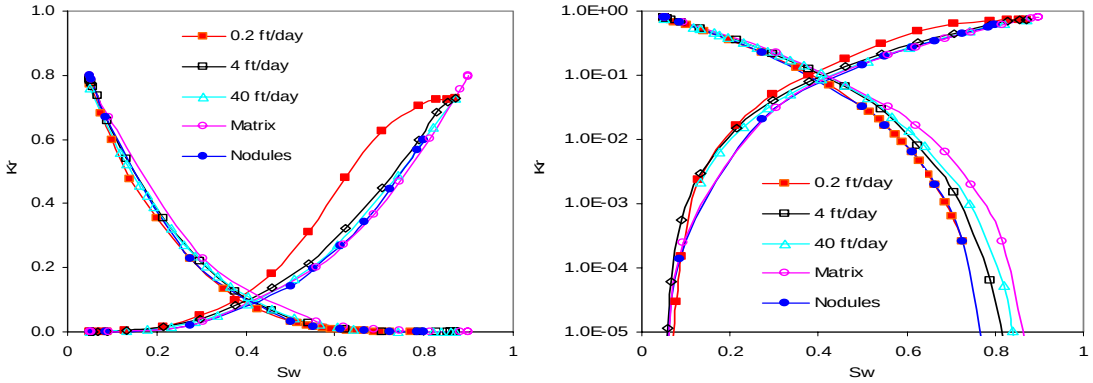

Figure 12: The upscaled imbibition oil and water relative permeability curves from steady-state experiments at three different rates. Left – data plotted in Cartesian scale; right – same data plotted in semi-logarithmic scale.

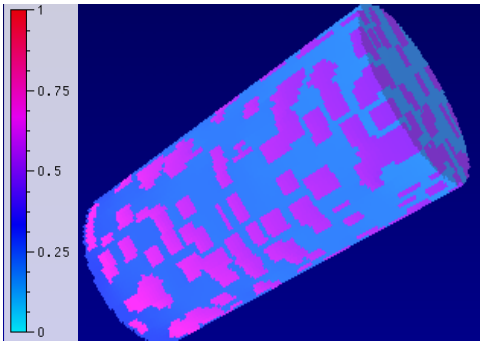

Figure 13: Remaining oil saturation (ROS) distribution after waterflooding a bioturbated model (at 0.4 ft/day).

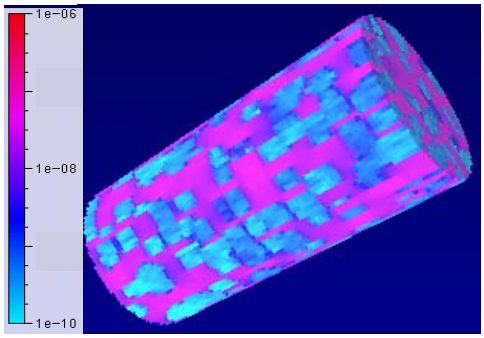

Figure 14: Capillary number (Nc) distribution after waterflooding a bioturbated model (at 0.4 ft/day).